

Unification of the phonon mode behaviour in semiconductor alloys

O. Pagès,* M. Kassem, A. Chafi, A. Nassour, S. Doyen and A. V. Postnikov

Laboratoire de Physique des Milieux Denses, Université Paul Verlaine – Metz,
1 Bd. Arago, F-57078 Metz, France

This work concludes a series of systematic re-examinations of the Raman/Infrared spectra of representative semiconductor alloys in the traditionally admitted classification of phonon mode behaviour, i.e. $\text{In}_{1-x}\text{Ga}_x\text{As}$ (1-bond \rightarrow 1-mode), $\text{In}_{1-x}\text{Ga}_x\text{P}$ (modified 2-mode) and presently $\text{ZnTe}_{1-x}\text{Se}_x$ (2-bond \rightarrow 1-mode), based on a crude description of the alloy disorder at the *macroscopic* scale in terms of the virtual crystal approximation (VCA). Here we show that the latter alloy obeys the same phonon mode behaviour as the former two, thereby a universal one, of a percolation type (1-bond \rightarrow 2-mode). The ‘VCA \rightarrow Percolation’ change of paradigm confers to vibrational spectroscopies the attractive privilege to provide natural insight into the alloy disorder at the unusual *mesoscopic* scale, with potential interest for the study of the long scale (self) organization in alloys, in general.

The key issue regarding mixtures is how to handle the substitutional disorder. For natural mixtures, of a forbidding complexity at the *microscopic* scale, a percolation-based approach was developed at the *mesoscopic* scale.¹ The central notion is the volume fraction of each constituent. Singularities in the physical properties are expected at the percolation thresholds, at which compositions the minor constituents coalesce into a continuum. Surprisingly, for those ideally-disordered mixtures that are usual semiconductor (SC) $\text{AB}_{1-x}\text{C}_x$ alloys (atoms in substitution on a regular lattice), made of the two interpenetrating A and (B,C) fcc sublattices, the virtual crystal approximation (VCA) seems sufficient, in first approximation. With this, each atom A is surrounded by four virtual B_{1-x}C_x atoms, i.e. the crystal is viewed at the *macroscopic* scale as a continuum (Fig. 1a). The physical properties are accordingly averaged. No singularity is expected in their dependence on x .

Here, we focus on the bond force constant (K) in SC alloys. K is sensitive to the bond distortion (bond length plus bond angles) required to accommodate the mismatch in the A-B and A-C bond lengths, and as such provides an integrated insight into the substitutional disorder.^(a) K is routinely probed by Raman and Infrared (IR) spectroscopies, via the frequency of the transverse optical (TO) phonon.^(b) The VCA for K leads to a 1-bond \rightarrow 1-mode TO behaviour, as accounted for by the modified-random-element-isodisplacement (MREI) model.² Only one adjustable parameter is needed per bond, i.e. the frequency of the impurity mode ω_{imp} – see Methods. The MREI-VCA supports a classification of the TO-Raman/IR data in terms of 2-mode (pure 1-bond \rightarrow 1-mode) (i), mixed-mode (2-bond \rightarrow 1-mode)

(ii) and dominant-plus-minor mixed-modes (modified-2-mode) (iii) – see Methods. Representative systems are $\text{In}_{1-x}\text{Ga}_x\text{As}$, $\text{ZnTe}_{1-x}\text{Se}_x$ and $\text{In}_{1-x}\text{Ga}_x\text{P}$, respectively (ref. 3). Elliott *et al.* (ref. 4) worked out a theoretical criterion within the coherent potential approximation

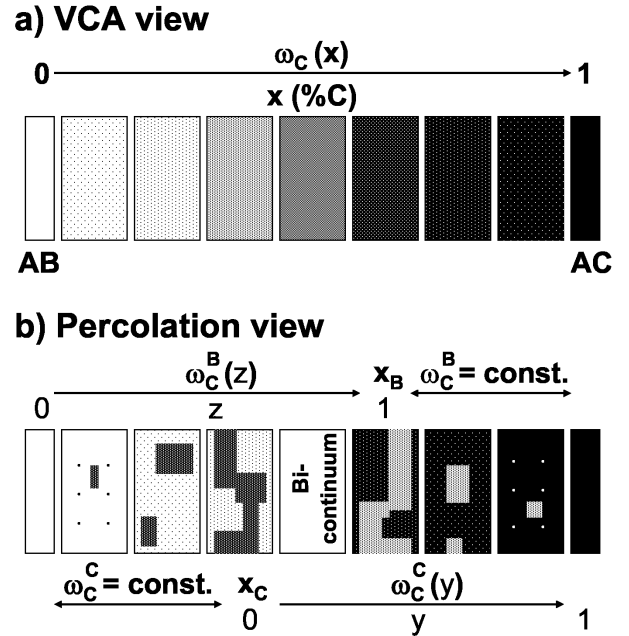


FIG. 1 Schematic views of a $\text{AB}_{1-x}\text{C}_x$ alloy according to the VCA (a) and percolation (b) approaches. We use a simple greyscale code. In the alloy the greyscale reinforces when the local composition becomes more like that of the corresponding pure crystal. A correlation with the dependence of the A-C TO-frequency (ω) on the actual alloy composition x (a) or on re-scaled alloy compositions y and z (b) is indicated. A similar description applies to the A-B TO-frequency. Subscript and superscript B (C) refer to the A-B (A-C) bond species and to the – pale – B-rich (– dark – C-rich) region, respectively. In case (b) critical behaviours occur at the A-C ($x_C=0.19$) and A-B ($x_B=0.81$) bond percolation thresholds.

*Author to whom correspondence should be addressed:
e-mail: pages@univ-metz.fr

(a) A simple rule is ‘the closer the atoms, the larger K ’.

(b) A TO mode in the Raman/IR spectra corresponds to out-of-phase vibrations of the A and (B,C) sublattices, perpendicular to the direction of propagation.

(CPA)^(c) that predicts type (ii) when the A-B and A-C optical bands overlap in the alloy, type (i) otherwise.^(d) The MREI-VCA (experimental) and Elliott-CPA (theoretical) classifications were found to be remarkably consistent, except for InGaP. From the Elliott-CPA criterion, InGaP should be of type (ii). However, careful analysis of the Raman/IR data reveals that even the accepted representative alloys we discuss do not fit into the MREI-VCA/Elliott-CPA classification.^(e) Our view is that the VCA misses the essence of the phonon behaviour in alloys. Recognizing the local character of K we conclude that the proper understanding of TO phonons requires insight into the topologies of the (B,C)-substituting species, which falls into the scope of the percolation site theory.⁸ Precisely, the apparent anomalies in InGa(As,P) could be explained within a so-called 1-bond \rightarrow 2-mode percolation model,⁹ introducing a description of an alloy at the *mesoscopic* scale, as a composite (Fig. 1b). Two adjustable parameters are required per bond, i.e. ω_{imp} plus the splitting Δ between like TO modes in the dilute limit – see Methods.

Here, we investigate whether the percolation scheme for InGa(As,P) is fortuitous, i.e. contingent upon the (Ga,In)-substituting species for some reason, or reflects a deeper – universal – reality by extending further to the representative system of the remaining class (ii), i.e. ZnTeSe. The perspective is a change of paradigm regarding the way to describe phonons in alloys.

Percolation picture for ZnSeTe

The context is favourable for the detection of a possible 1-bond \rightarrow 2-phonon behaviour in ZnTeSe. Indeed the lattice mismatch in ZnTeSe is similar to that of InGa(As,P), i.e. $\sim 7\%$, so that similar lattice distortions can be ex-

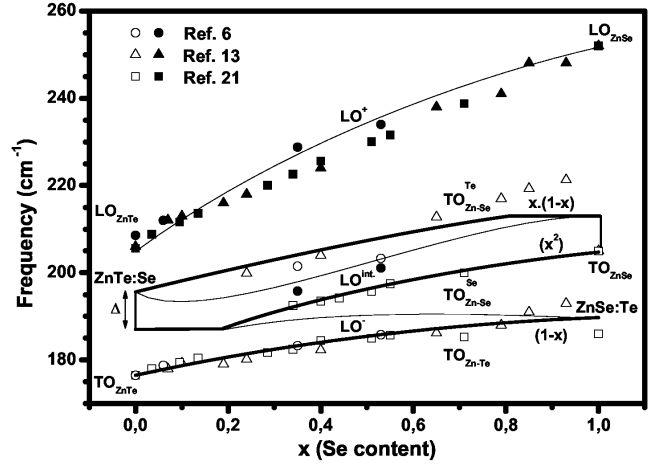


FIG. 2 TO (thick lines)/LO (thin lines) percolation picture for $\text{ZnTe}_{1-x}\text{Se}_x$. Representative sets of TO (open symbols) and LO (filled symbols) frequencies taken from the literature, as indicated, are added. The fraction of bonds corresponding to each TO branch is indicated on the right side. ZnTe:Se (ZnSe:Te) is the notation for the impurity mode of Se (Te) in ZnTe (ZnSe).

pected, and thereby also similar phonon properties.^(f) In fact, already three decades ago Artamonov *et al.* (ref. 12) did mention an ‘evident analogy’ between the phonon mode behaviours of InGaP and ZnTeSe. Also, recently Yang *et al.* (ref. 13) proposed to re-classify ZnTeSe as a type (iii) system, not as a type (ii). Altogether this suggests that a InGaP-like version of the percolation model should apply to ZnTeSe.

Representative sets of optical-phonon frequencies in ZnTeSe, taken in the literature, are displayed in Fig. 2. In the discussion of the phonon mode behaviour, we focus on the TO modes, the longitudinal optical [LO, note (d)] modes follow. The data indicate three equally spaced TO modes in the range 180–200 cm^{-1} , that blue-shift when the Se content increases. We propose a three-oscillator [1 (Zn-Te), 2 (Zn-Se)] version of the percolation model, with a unique $\text{TO}_{\text{Zn-Te}}$ branch below a well-resolved Zn-Se TO double-branch (see details below). Bonds are longer (shorter) in environments rich of the shorter (longer) bonds,^{9,14} which reduces (enlarges) the TO frequency. So, the middle and upper TO branches are due to Zn-Se vibrations in the Se- and Te-rich regions, accordingly labelled as $\text{TO}_{\text{Zn-Se}}^{\text{Se}}$ and $\text{TO}_{\text{Zn-Se}}^{\text{Te}}$. The (ω_{imp} , Δ) values for the Zn-Te and Zn-Se bonds are ($\sim 189 \text{ cm}^{-1}$, $\sim 0 \text{ cm}^{-1}$) and ($\sim 195 \text{ cm}^{-1}$, $\sim 8 \text{ cm}^{-1}$), respectively.

^(c) As the CPA is well-suited mainly for the treatment of low concentration of simple defects in otherwise perfect media, the Elliott-CPA criterion aims at deriving the whole phonon mode behaviour of an alloy from its behaviour in the dilute limits.

^(d) Here, the optical bands are simply build up by linear extrapolations of the frequencies of the transverse optical (TO) and longitudinal optical (LO) modes in the pure crystal onto the related impurity frequency. The LO phonon corresponds to out-of-phase vibrations of the A and (B,C) sublattices along the direction of propagation. In a polar crystal it differs from a TO mode in that it carries a long range polarization field \vec{E} due to the ionicity of the bond. In a pure crystal this is responsible for an additional coulombian restoring force, with the result that the LO mode vibrates at a higher frequency than the TO mode. In an alloy the LO mode is a more complicated issue, as discussed at the end of the manuscript.

^(e) There are three features in the TO Raman spectra of InGaAs, instead of two.⁵ Also, the IR spectra of ZnTeSe exhibit two clear resonances, not only one.⁶ At last, the minor mode of InGaP was identified by *ab initio* calculations as a pure Ga-P mode, not as a (In-P,Ga-P)-mixed mode.⁷

^(f) Further, the dispersion of the TO mode is small in ZnSe ($\sim 6 \text{ cm}^{-1}$) and ZnTe ($\sim 8 \text{ cm}^{-1}$) (ref. 10), so that even small fluctuations in the local bond distortion may generate fluctuations in the TO frequency larger than the dispersion, thereby giving rise to phonon localization, i.e. to different TO modes in the Raman/IR spectra.¹¹

The ω_{imp} values were estimated by relying on thorough extended X-ray absorption fine structure (EXAFS) measurements of bond length in ZnTeSe.¹⁵ The shift of an impurity mode with respect to the TO mode in the pure crystal was inferred from the related difference in bond length δ via the TO mode Grüneisen parameter γ in the pure crystal, by using Eq. (2) in ref. 9. For the Zn-Te (Zn-Se) bond, δ and γ are 2.480–2.452 Å (2.600–2.643 Å) and 1.4 (1.7), according to refs. 15 and 16, respectively.

Now, we turn to Δ . The lower set of TO data is attached to the limit ($x \sim 0.1$) Zn-Te frequencies at its two ends, indicating an apparent 1-bond \rightarrow 1-mode MREI behaviour for the Zn-Te bond, which comes to $\Delta_{\text{Zn-Te}} \sim 0 \text{ cm}^{-1}$. The remaining sets of TO data share quasi-symmetrically on each side of the limit Zn-Se frequencies, indicating a well-resolved 1-bond \rightarrow 2-mode type behaviour for the Zn-Se bond, i.e. a finite $\Delta_{\text{Zn-Se}}$ value. This was adjusted to $\sim 8 \text{ cm}^{-1}$ by fitting a rescaled-MREI curve to the data in the continuum regime of the dominant $\text{TO}_{\text{Zn-Se}}^{\text{Se}}$ branch at large Se content. The remaining pieces of the Zn-Se double-branch, i.e. the two dispersion regimes plus the rescaled-MREI curve in the continuum regime of the $\text{TO}_{\text{Zn-Se}}^{\text{Te}}$ branch, were directly inferred – see Methods.

The agreement between the TO (thick lines) / LO (thin lines) theoretical curves and the data is rather good, in spite of the simplicity of our model. Slight discrepancy exists with respect to the $\text{TO}_{\text{Zn-Se}}^{\text{Te}}$ branch in the Te-dilute limit, where the mode becomes weak and hard to detect. In Fig. 2 the [Zn-Te, (Zn-Se)^{Se}, (Zn-Se)^{Te}] TO-frequency information is completed on the TO-intensity side by the terms within brackets – see Methods.

(TO,LO) Raman lineshapes

All the ingredients are there to calculate the TO and LO Raman lineshapes of random ZnTeSe. We use the generic expression of the Raman cross section given by Eq. (1) in ref. 9. In a form restricted to the second member it gives access to the TO modes; in full it provides the LO modes. We use a classical form of the dielectric function, generalized to three harmonic oscillators. For a direct comparison with the Raman spectra we take Zn-Se and Zn-Te phonon dampings that scale like in pure crystals, i.e. 3:1, as inferred from the full widths at half maximum of the LO Raman lines (compare Figs. 1 in refs. 17 and 18). The remaining ($C_{\text{F-H}}$, ϵ_{∞} , TO-LO) values for the pure ZnSe and ZnTe crystals, with the usual notation,⁹ are (−0.56, 5.75, 206–252 cm^{-1}) and (−0.32, 7.20, 176–206 cm^{-1}), respectively.^(g) The resulting three-mode TO and LO Raman lineshapes are shown in Fig. 3. We use small dampings for the Zn-Te (1 cm^{-1})

and Zn-Se (3 cm^{-1}) modes, for a clear overview of the whole collection of oscillators.

First, we discuss briefly the LO modes (thin lines in Figs 2 and 3). In a multi-wave system, such as an alloy, the electric field \vec{E} is well-known to act as a carrier of coherence,²⁰ that makes LO modes [see note (d)] a complicated issue.⁹ This is especially true in ZnTeSe because the Zn-Se and Zn-Te oscillators are so close. Therefore the individual $\text{LO}_{\text{Zn-Te}}$, $\text{LO}_{\text{Zn-Se}}^{\text{Se}}$ and $\text{LO}_{\text{Zn-Se}}^{\text{Te}}$ modes (not shown) do \vec{E} -couple strongly, with the result that the available oscillator strength, independently of its origin, i.e. ZnSe- or ZnTe-like, is almost fully channelled into a ‘giant’ LO^+ mode at high frequency. This exhibits a model type (ii) behaviour, as is obvious in Fig. 3, certainly the origin of the MREI-VCA classification of ZnTeSe. Residual $\text{LO}^{\text{int.}}$ and LO^- modes, in the sense of decreasing frequencies, are driven back towards the TO modes.

On the basis of Fig. 3, we re-assign the presumed unique TO mode in the Raman/IR spectra of ZnTeSe as the sum of close $\text{TO}_{\text{Zn-Te}}$ and $\text{TO}_{\text{Zn-Se}}^{\text{Se}}$ modes. In fact the bi-modal character was already obvious in the Raman spectra recorded by Artamonov *et al.* (ref. 21). The two modes exhibit antagonist strength variations when the composition changes, and have similar heights at $\sim 70\%$ Se, consistently with experimental observations.²¹ An additional minor LO-TO inverted oscillator within the main TO-LO band, evidenced by using IR reflectivity,⁶ is assigned as the $\text{LO}^{\text{int.}}$ – $\text{TO}_{\text{Zn-Se}}^{\text{Te}}$ band. The LO-TO in-

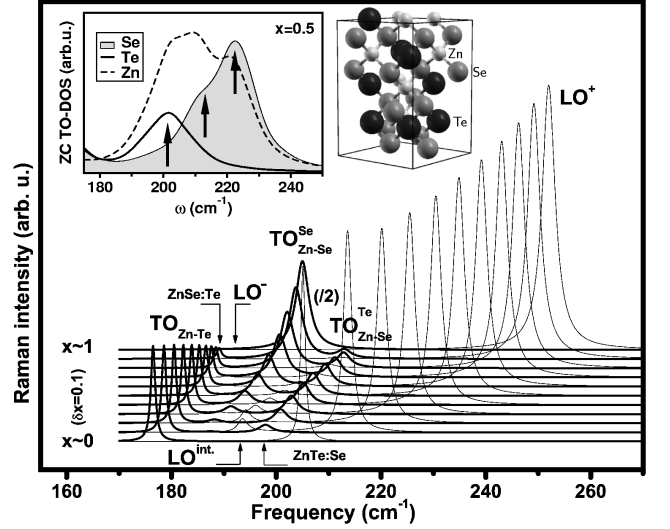


FIG. 3 TO (thick lines) and LO (thin lines) Raman lineshapes calculated for $\text{ZnTe}_{1-x}\text{Se}_x$ from Fig. 2 by using Zn-Se and Zn-Te phonon dampings that scale as in the pure crystals, i.e. 3:1. The bottom LO mode is divided by 2, as indicated. The ZC TO-DOS obtained per atom at $x \sim 0.5$ by using uniformly-damped Zn, Se and Te oscillators, is shown in the inset for comparison, together with the corresponding quasi-random supercell. There, the arrows indicate a three-oscillator behaviour.

^(g) $C_{\text{F-H}}$ is taken as the ratio of the ionic to electronic parts of the static electro-optic effect, as calculated by Shih *et al.* (ref. 19).

verted splitting is large at intermediate composition, and further increases with the Te content, as evidenced by Burlakov *et al.* (ref. 6). Then it vanishes in the dilute limits, as observed by Yang *et al.* (ref. 13). In brief, all the ‘anomalous’ features in the Raman/IR spectra of ZnTeSe find a natural assignment in terms of allowed modes within the percolation picture, on a quantitative basis. Actually, there is a quasi-perfect analogy between the phonon mode behaviours of ZnTeSe and InGaP (ref. 9).

To secure a basis of our discussion on TO modes we provide independent *ab initio* insight into the TO density of states (TO-DOS) at the zone-center (ZC), that compares directly to the Raman signal, in a fully-relaxed 32-atom supercell (volume and internal coordinates) at the representative composition $x \sim 0.5$. The Se and Te atoms are equally distributed over all substituting planes, as expected in a random alloy. We apply the plane-wave pseudopotential method within the density functional theory and the local density approximation (LDA), and a linear response technique.²² The ZC TO-DOS obtained per atom for uniformly-damped Zn, Se and Te oscillators ($\sim 10 \text{ cm}^{-1}$) are displayed in the inset of Fig. 3, together with the supercell. As expected, three equidistant oscillators spaced by $\sim 10 \text{ cm}^{-1}$, with similar strengths, i.e. a ZnTe-like below two ZnSe-like ones (refer to the arrows in the inset of Fig. 3), show up. A slight overall blue-shift of the ZC TO-DOS with respect to the corresponding Raman lineshape ($\sim 20 \text{ cm}^{-1}$) is due to a well-known overbinding in LDA. We have checked that the interplay between the frequencies and strengths of the three oscillators in the ZC TO-DOS and the phenomenological TO Raman lineshapes are consistent over the whole composition domain.

Percolation vs. Elliott-CPA and MREI-VCA

The percolation schemes for InGaAs, InGaP and ZnTeSe are schematically reproduced in Fig. 4. Only the TO branches are shown, for clarity, while simplifying the continuum regimes to straight lines – see Methods. There is an obvious analogy between the three schemes, indicating that the traditional MREI-VCA/Elliott-CPA classification has, in fact, no *raison d’être*.

Still, the percolation schemes must be consistent with the latter classification, which we discuss now. In both InGaAs and InGaP, the impurity modes stay out of the parent TO-LO bands, so that the Ga- and In-related TO-LO bands in the alloy (shaded areas in Figs 4a and 4b) do not overlap. In contrast the Zn-Se and Zn-Te TO-LO bands do overlap in ZnTeSe (refer to the over-shaded area in Fig. 4c). This is consistent with the Elliott-CPA classification of InGa(As,P) and ZnTeSe as types (i) and (ii), respectively. The percolation schemes are also consistent with the MREI-VCA classification. It is just a matter of regrouping close individual/double TO branches as shown by ovals in Fig. 4. The usual terminology of indi-

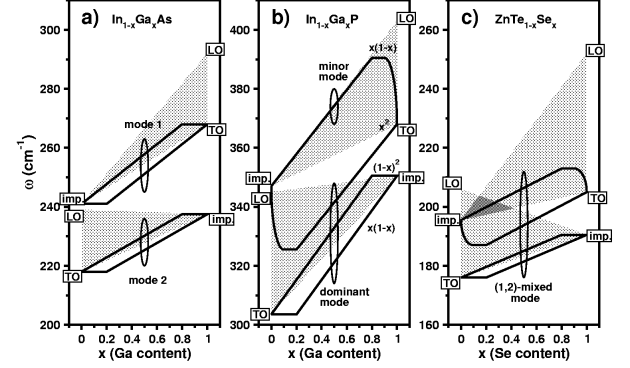


FIG. 4 Simplified 1-bond \rightarrow 2-mode TO (thick lines) percolation schemes of InGaAs (a), InGaP (b) and ZnTeSe (c). The generic fraction of bonds corresponding to each TO branch is indicated in part (b). The bond-related optical bands simply obtained by linear convergence of the parent TO and LO frequencies onto the related impurity frequencies are shown as shaded areas.

vidual modes [(i), Fig. 4a], dominant-plus-minor modes [(ii), Fig. 4b] and mixed-mode [(iii), Fig. 4c] comes out naturally.

A probable reason why differences in the detail of the phonon mode behaviours of InGaAs, InGaP and ZnTeSe were previously mistaken for differences in the principles of the phonon mode behaviours lies in an implicit, but wrong, assumption that the TO and LO modes behave similarly in an alloy. In particular, in the LO symmetry a strong \vec{E} -coupling occurs between the like LO modes that come from the same double-branch, because these refer to the same bond species and as such have close frequencies. The result is that the actual 1-bond \rightarrow 2-mode behaviour visible in the TO symmetry, supporting a description of the phonon mode behaviour at the *mesoscopic* scale on a percolation basis, is literally rubbed out in the LO symmetry. What is left is an apparent 1-bond \rightarrow 1-mode LO behaviour, encouraging a more crude description at the *macroscopic* scale according to the MREI-VCA. Due to this TO vs. LO duality, any attempt to explain the TO and LO modes in an alloy on the same intuitive basis is damned to fail. Simplicity arises by focusing on TO modes; LO modes follow.

In brief, we show that ZnTeSe obeys the 1-bond \rightarrow 2-phonon percolation model, as InGaAs and InGaP do. We propose a three-oscillator [1 Zn-Te, 2 Zn-Se] version, supported by existing EXAFS data and home-made *ab initio* phonon calculations. This leads to unification of the traditional MREI-VCA/Elliott-CPA classification into a single class covered by the percolation model. It emerges that even those ideally-disordered systems that are the usual SC alloys can not escape a description of some of their very basic physical properties via a percolation concept. As such, they do not differ fundamentally from other mixtures, contrarily to a broadly accepted assumption. On the practical side, this work reveals that

vibrational spectroscopies provide natural insight (non destructive and contactless) into the alloy disorder at the unusual mesoscopic scale, which is hardly achieved otherwise. This offers an attractive perspective for the study of the long scale (self-) organization in alloys, be it local ordering⁹ or anti-clustering.²³

The authors acknowledge support from the IFCPAR (N° 3204-1) and the CINES (N° pli2623).

Methods

MREI-VCA (TO) model: The VCA for a bond-related property, such as K , comes to a picture where the bond is immersed into a continuum whose properties are smoothly x -dependent (Fig. 1a). The bonds of like species are all equivalent, thereby contributing to a unique TO-Raman/IR mode. The intensity scales as the corresponding fraction of bonds, and when x changes the mode shifts smoothly between the parent and impurity limits. No singularity is expected. A short (long) impurity bond is tensed (compressed) in a matrix with a large (small) lattice constant, which reduces (enlarges) K , with concomitant impact on ω_{imp} [see note (a)]. Generally ω_{imp} remains close to the parent TO-frequency, because each bond tends to keep its natural bond length in an alloy. So, the trend in a ‘TO-frequency vs. x ’ plot is that the A-B and A-C TO branches remain quasi-parallel, with slight, but finite, slopes.

TO-based MREI-VCA classification: Two main types of TO behaviour proceed from the MREI-VCA: (i) If the parent TO frequencies are much distinct, the alloy exhibits well-separated A-B and A-C TO branches, corresponding to a typical 1-bond→1-mode behaviour. (ii) If the parent TO frequencies are close enough, the A-B and A-C TO branches merge into an apparent 2-bond→1-mode behaviour with a unique (A-B, A-C)-mixed TO mode that has quasi-stable strength, and shifts regularly between the parent TO modes. There seems to exist an intermediary-type behaviour, referred to as (iii), with two (A-B, A-C)-mixed TO modes, i.e. a dominant one of type (ii), plus a minor one that does not allow to fully discard type (i). While the MREI-VCA model fully accounts for types (i) and (ii), it can not account for type (iii), even qualitatively.

Percolation (TO) model: This distinguishes between vibrations of like bonds within the naturally-formed B-rich and C-rich regions (Fig. 1b), the result of different local bond distortions. In a ‘TO-frequency vs. x ’ plot, this results in a splitting of each MREI-like TO branch into a symmetrical double-branch, attached at its two

ends to the parent and impurity modes. The strength of each ‘sub-mode’ scales as the corresponding B-rich (x) or C-rich region ($1-x$). Singularities in the TO-frequency occur at the bond percolation thresholds (PT’s), where the minor A-B ($x_B=0.19$) or A-C ($x_C=0.81$) bonds become connected throughout the crystal. Below the PT, the minor region consists of a dispersion of finite clusters with similar structures, which generates invariance in the TO-frequency. Above the PT, the finite clusters coalesce into a continuum whose local composition turns smoothly x -dependent, as does the TO-frequency. A rescaled-MREI approach applies where the continuum, viewed as a pseudo-alloy, takes an apparent composition varying from 0 to 1 over its domain of existence (refer to y, z in Fig. 1b).

Ab initio protocol for a self-consistent percolation model:

For straightforward data-independent (Raman/IR) insight into ω_{imp} and Δ in any zincblende alloy we propose here a simple protocol based on *ab initio* bond length/phonon calculations in prototype fully-relaxed supercells at the dilute limits. We use 64-atom supercells, that are well-converged in size for such purpose.²⁴ The calculations are performed by using the computer code SIESTA within the LDA (ref. 25).

To access ω_{imp} , we use a supercell containing a single impurity ($\sim 3\%$ imp.). This is the ultimate configuration that refers to an impurity in the region rich of the other substituting species. We search for the impurity bond length, and we estimate ω_{imp} via γ as usual (see main text). A direct calculation of the impurity frequency $\omega_{\text{imp}}^{\text{calc.}}$ does not help here, due to the effective overbinding in LDA.

To access Δ we use a supercell containing two neighbouring substitutional impurities. This pair forms the germ of the impurity-rich region, i.e. the ultimate configuration that refers to an impurity staying in its own environment. We search for the frequency of the phonon mode along the chain of the two impurity bonds, referred to as $\omega_{\text{pair}}^{\text{calc.}}$, and Δ is estimated as $|\omega_{\text{imp}}^{\text{calc.}} - \omega_{\text{pair}}^{\text{calc.}}|$. The systematic error due to LDA is thus eliminated.

We have checked that the theoretical and experimental ($\omega_{\text{imp}}, \Delta$) values for random InGaAs, InGaP and ZnTeSe, and also (Zn,Be)-chalcogenides that exhibit a unusually large contrast in the bond properties, agree within $\sim 5\%$. This validates the *ab initio* protocol. Together with it, our phenomenological percolation model forms a self-consistent model for the calculation of the 1-bond→2-mode Raman/IR behaviour in any zincblende alloy. This can be viewed as a sophistication to the mesoscopic scale of the traditional 1-bond→1-mode MREI model, that operates at the macroscopic scale.

References

1. De Gennes, P. G., *Scaling concepts in Polymer Physics* (Cornell University Press, Ithaca and London, 1979)
2. Chang, I.F. & Mitra, S.S. Long wavelength optical phonons in mixed crystals. *Adv. Phys.* **20**, 359 (1971)
3. Mascarenhas, A., Cheong, H. M., Seong, M. J. & Alsina, F., in *Spontaneous Ordering in Semiconductor Alloys* (ed. Mascarenhas, A., Kluwer Academics/Plenum Publishers, New York, 2002), p. 391
4. Elliott, R. J., Krumhansl, J. A., & Leath, P. L. The theory and properties of randomly disordered crystals and related physical systems. *Rev. Mod. Phys.* **46**, 465 (1974)
5. Groenen, J., Carles, R., Landa, G., Guerret-Piécourt, C., Fontaine, C. & Gendry M. Optical-phonon behavior in $\text{Ga}_{1-x}\text{In}_x\text{As}$: The role of microscopic strains and ionic plasmon coupling. *Phys. Rev. B* **58**, 10452 (1998)
6. Burlakov, V. M., Litvinchuk, A. P. & Pyrkov, V. N. Infrared reflection spectra of $\text{ZnTe}_{1-x}\text{Se}_x$ solid solutions. *Sov. Phys. Solid State* **27**, 131 (1985)
7. Ozoliņš, V. & Zunger, A. First-principles theory of the evolution of vibrational properties with long-range order in GaInP_2 . *Phys. Rev. B* **57**, R9404 (1998)
8. Stauffer, D., *Introduction to Percolation Theory* (Taylor and Francis, London, 1985)
9. Pagès, O., Chafi, A., Fristot, D. & Postnikov, A. V. (Ga,In)P: A standard alloy in the classification of phonon mode behavior. *Phys. Rev. B* **73**, 165206 (2006)
10. Rajput, B. D. & Browne, D. A. Lattice dynamics of II-VI materials using the adiabatic bond-charge model. *Phys. Rev. B* **53**, 9052 (1996)
11. Cardona, M., Etchegoin, P., Fuchs, H. D. & Molinàs-Mata, P. Effect of isotopic disorder and mass on the electronic and vibronic properties of three-, two- and one-dimensional solids. *J. Phys.: Condens. Matter* **5**, A61 (1993)
12. Artamonov, V. V., Ya Valakh, M. & Vitrikhovskii, N. I. Influence of a resonance interaction on the variation of the phonon spectrum in $\text{ZnTe}_{1-x}\text{Se}_x$ crystals. *Sov. Phys. Solid State* **21**, 1015 (1979)
13. Yang, C. S., Chou, W. C., Chen, D. M., Ro, C. S. & Shen J. L. Lattice vibrations of $\text{ZnSe}_{1-x}\text{Te}_x$ epilayers grown by molecular-beam epitaxy. *Phys. Rev. B* **59**, 8128 (1999)
14. Silverman, A., Zunger, A., Kalish, R. & Adler, J. Atomic-scale structure of disordered $\text{Ga}_{1-x}\text{In}_x\text{P}$ alloys. *Phys. Rev. B* **51**, 10795 (1995)
15. Pellicer-Porres, J., Polian, A., Segura, A., Muñoz-Sanjosé, V., Di Cicco, A. & Traverse, A. X-ray-absorption fine-structure study of $\text{ZnSe}_x\text{Te}_{1-x}$ alloys. *J. Appl. Phys.* **96**, 1491 (2004)
16. Trommer, R., Müller, H., Cardona, M. & Vogl, P. Dependence of the phonon spectrum of InP on hydrostatic pressure. *Phys. Rev. B* **21**, 4869 (1980)
17. Pagès, O., Ajjoun, M., Laurenti, J. P., Bormann, D., Chauvet, C., Tournié, E. & Faurie, J. P. Raman study of $\text{ZnBe}_{1-x}\text{Se}_x$ alloy (100) epitaxial layers. *Appl. Phys. Lett.* **77**, 519 (2000)
18. Pagès, O., Tite, T., Bormann, D., Maksimov, O. & Tamargo, M. C. Percolation behaviour in the Raman spectra of ZnBeTe alloy. *Appl. Phys. Lett.* **80**, 3081 (2002)
19. Shih, C.-C. & Yariv, A. A theoretical model of the linear electro-optic effect. *J. Phys. C: Solid State Phys.* **15**, 825 (1982)
20. Fano, U. A common mechanism of collective phenomena. *Rev. Mod. Phys.* **64**, 313 (1992)
21. Artamonov, V. V., Sidorenko, V. I. & Yaremko, A. M. Manifestation of the interference of vibrational states in the combinational scattering spectra of $\text{ZnTe}_x\text{Se}_{1-x}$ mixed crystals. *Ukr. Fiz. Zh.* **28**, 42 (1983)
22. Giannozzi, P., De Gironcoli, S., Pavone, P. & Baroni, S. Ab initio calculation of phonon dispersions in semiconductors. *Phys. Rev. B* **43**, 7231 (1991)
23. Chafi, A., Pagès, O., Postnikov, A.V., Gleize, J., Sallet, V., Rzepka, E., Li, L. H., Jusserand, B. & Harmand, J. C. Combined Raman study of InGaAsN from the N-impurity and InGaAs-matrix sides. *Appl. Phys. Lett.* **91**, 51910 (2007)
24. Teweldeberhan, A. M. & Fahy, S. Effect of indium-nitrogen bonding on the localized vibrational mode in $\text{In}_y\text{Ga}_{1-y}\text{N}_x\text{As}_{1-x}$. *Phys. Rev. B* **73**, 245215 (2006)
25. Soler, J. M., Artacho, E., Gale, J. D., García, A., Junquera, J., Ordejón, P. & Sánchez-Portal, D. The SIESTA method for *ab initio* order- N materials simulation. *J. Phys.: Condens. Matter* **14**, 2745 (2002)